Journal Pre-proof

Experimental study of chemical evolution and isotope fractionation of Cl and Br in pore water expelled during strong clay compaction

Jessica Strydom, Jérôme Sterpenich, Dragan Grgic, Antonin Richard, Hans G.M. Eggenkamp, Pierre Agrinier, Pascale Louvat, Régine Mosser-Ruck, Patrick Gaire, Eric C. Gaucher

Please cite this article as: Strydom, J., Sterpenich, Jéô., Grgic, D., Richard, A., Eggenkamp, H.G.M., Agrinier, P., Louvat, P., Mosser-Ruck, Ré., Gaire, P., Gaucher, E.C., Experimental study of chemical evolution and isotope fractionation of Cl and Br in pore water expelled during strong clay compaction, *Applied Geochemistry* (2022), doi: https://doi.org/10.1016/j.apgeochem.2022.105274.

1 **Experimental study of chemical evolution and isotope fractionation of Cl and Br in pore**

2 **water expelled during strong clay compaction**

3

4 Jessica Strydom[a], Jérôme Sterpenich[a], Dragan Grgic[a], Antonin Richard[a], Hans G. M.

5 Eggenkamp[b,d], Pierre Agrinier[b], Pascale Louvat[b], Régine Mosser-Ruck[a], Patrick Gaire[a], Eric

6 C. Gaucher[c,e]

7

8 [a]Université de Lorraine, CNRS, GeoRessources, CREGU, F-54000 Nancy, France.

9 [b]Université Paris Cité, Institut de Physique du Globe de Paris, 1, rue Jussieu - 75238 Paris

10 cedex 05, France

11 [c]Total CSTJF, Avenue Larribau, Pau, F-64000, France

12 [d]Mathematisch-Naturwissenschaftliche Fakultät, FB Geowissenschaften, Eberhard Karls

13 Universität Tübingen, Schnarrenbergstraße 94-96, D-72076 Tübingen, Germany

14 [e]Institute of Geological Sciences, University of Bern, Baltzerstrasse 1+3, CH-3012 Bern,

15 Switzerland

16

17 Corresponding author's email: jerome.sterpenich@univ.lorraine.fr

24 **ABSTRACT**

25

26 In sedimentary basins, clay compaction by burial can lead to fluid overpressure and is suspected

27 to also generate fresh waters, but few geochemical tracers are available to assess this process

28 both qualitatively and quantitatively. Our objective was to carry out experiments on the

29 chemical - and halogen (Cl, Br) isotope evolutions of pore water expelled during clay

30 compaction. For this, the smectite-rich bentonite MX80 and an illite-rich marl (Sainte-Suzanne)

31 were equilibrated with ocean water. During two compaction experiments under high fluid

32 pressure (45 MPa), mechanical stress (up to 150 MPa) and temperature (up to 150 °C), it was

33 found that the chemistry and isotope behavior is considerably different between the swelling

34 clay and the non-swelling clay.

35 We saw a general decrease of the cat- and anion concentrations in the expelled water, for

36 swelling clay while its concentration slightly increases in the remaining pore fluid. This was

37 not the case for non-swelling clay. More freshening of the expelled water occurred during the

38 compaction at higher temperature.

39 We also observed a larger range of isotopic variation for Br (δ^{81}Br from 0.9‰ up to 1.5‰) than

40 for Cl (δ^{37}Cl from -0.5‰ to -0.1‰) in the compaction experiments. During the compaction of

41 illite-rich marl, no significant variation of Cl isotope (δ^{37}Cl close to 0‰) was observed while

42 the δ^{81}Br value of the expelled water showed the same general increase (from 0.9 ‰ up to

43 1.5‰) as during the compaction of smectite-rich bentonite.

44 We observed limited mineralogical transformations in terms of dissolution/precipitation

45 processes. Therefore the surface chemistry of the clay in combination with decreasing porosity,

46 in part, drive the anion and isotope evolution. We propose that significant retention of Cl and

47 Br in the pore water of the compacted smectite-rich bentonite is indicative of ultrafiltration and

48   that that Cl and Br isotopes are promising tracers to consider when tracking the origin of low-

49   salinity formation waters in sedimentary basins.

50

51
52   **1. INTRODUCTION**

53

54   Among the processes explaining fluid overpressure in sedimentary basins, the clay

55   compaction is one of the most significant. Clay compaction produces fresh water by the

56   physical process of ultrafiltration (Coplen and Hanshaw, 1973; Kharaka and Berry, 1973;

57   Haydon and Graf, 1986; Phillips and Bentley, 1987; Demir, 1988). The microstructure of the

58   clay rocks creates a very tortuous and electrically charged pore network inducing long

59   pathways and ionic repulsions trapping the ions in the clay rocks (Melkior et al., 2009).

60   Recently, two types of water produced during burial of clay formations were clearly described

61   by Tremosa et al. (2020). The first is produced by mechanical compaction when adsorbed

62   water layers are expelled. The second is produced by the mineralogical transformation of the

63   clays due to the increasing temperature. These two types of water dilute the former formation

64   waters. The term formation water describes water that saturates sedimentary rocks (among

65   them deep oil or gas reservoir rocks).

66   Migration of free-flowing formation water is an important factor in mass movement/transport

67   and diagenesis due to the inevitable chemical reactions with rocks along its migration path

68   Bethke and Marshak (1990). Studying formation waters is beneficial to understand the

69   original source of the waters, which could potentially link to the origin of the hydrocarbon

70   resources, the dynamics of low temperature geothermal systems and the formation of basin-

71   hosted mineral deposits Garven (1995). Formation waters can range from very saline to

72   remarkably fresh (low salinity or dilute) Solley and Chase (1983); Carpenter (1978); Hanor

73   (1987). Dilution or freshening of formation waters are attributed to;

74

75   1. Ultrafiltration (the relative retardation of solutes with respect to flowing solution when

76   passing through fine grained material

77   2. Condensate water (water produced from the condensation of water vapor present in

78   hydrocarbon gas reservoirs when the pressure is reduced during production)

79   3. Mixing with external fluids (meteoric water or diluted continental waters (rivers,

80   lakes))

81   4. Water-rock interactions

82   5. Clay mineral transformation/dehydration.

83

84 The hydrophilic and unreactive nature of chloride and bromide ions causes them to remain in

85 solution with very little incorporation into minerals (Davis et al., 1998; Worden, 1996).

86 Therefore, by studying Cl and Br anions as tracer conservative elements, one can follow the

87 fluid transport without much interference from water-rock interactions with the exception of

88 evaporates and organic matter (Richard et al., 2011; Kendrick et al., 2011; Pusch et al., 1990).

89 Because dissolved Cl and Br are so unreactive, it is also interesting to consider their stable

90 isotopes to understand what physical processes are influencing the fluid evolution. The stable

91 isotopes of both chlorine (^{35}Cl and ^{37}Cl) and bromine (^{79}Br and ^{81}Br) are fractionated by

92 natural and anthropogenic processes during their cycling between reservoirs. Stable isotope

93 ratios of Cl have been used to describe various physical processes that could have contributed

94 to formation water composition, including salt precipitation (Eggenkamp et al., 1995), ion

95 filtration (Phillips and Bentley, 1987), ion exchange (Musashi et al., 2004) and diffusion

96 (Eggenkamp and Coleman, 2009; Beekman et al., 2011). With fewer focused studies, the

97 behavior and application of Br stable isotope ratios is still not well understood (Shouakar-

98 Stash et al., 2007; Stotler et al., 2010). From previous literature, we know that the δ^{37}Cl

99 values of formation waters are usually negative and can vary significantly, down to -8‰

100 (Agrinier et al., 2019). From the few studies that have measured the isotopic ratios of Br in

101 formation waters, the δ^{81}Br values are mostly positive and vary up to +4‰ (Eggenkamp,

102 2014a). Both being halogens, Cl and Br have originally been assumed to show similar type of

103 isotopic variations. As the capabilities to measure Cl and Br isotopes have developed, it has

104 become clear that the stable isotopes of these anions fractionate differently despite their

105 similar chemical behavior. The fractionation of Cl isotopes by the process of diffusion has

106 been clearly illustrated in fine-grained low-porosity clay-rich materials (Kaufmann et al.,

107 1984; Phillips and Bentley, 1987; Lavastre et al., 2005). There seems to be a decreasing trend

108 for δ^{37}Cl with increasing depth (Agrinier et al., 2019, 2021). The fractionation of Br isotopes

109 due to diffusion has only been studied experimentally where it has been shown to correlate

110 with the diffusion of Cl (Eggenkamp and Coleman, 2009). It has been assumed previously

111 that due to the larger ionic radius and higher atomic mass, Br isotope fractionation should be

112 roughly half as large as Cl isotope fractionation (Eggenkamp (2014b)). δ^{81}Br trends with

113 increasing depth have not been studied. Interestingly, comparing published δ^{37}Cl and δ^{81}Br

114 values of natural formation waters, those samples with very negative Cl isotope ratios often

115 show surprisingly positive Br isotope values. It was suggested that these values might be the

116 result of ion filtration through semi-permeable clay membranes as a consequence of clay

117 surface charges (Tournassat and Appelo, 2011; Coplen and Hanshaw, 1973; Kharaka and

118 Berry, 1973; Campbell, 1985).

119 For this study, we are experimentally investigating ion filtration effects on ocean water by

120 means of a high pressure and temperature compaction experiment. It has been specifically

121 designed to extract pore water volumes large enough to measure chlorine and bromine stable

122 isotope composition, together with the evolution of pore water chemistry during stepwise

123 pressure and temperature increases, in order to follow the effect of clay compaction. We

124 compare two distinctly different clay-rich materials. The first, MX80, is a well-studied and

125 well-characterized clay with high content of swelling clay minerals (smectite). The second

126 material used is the Sainte Suzanne marl (SSM) from the Aquitaine basin (France) and is of

127 interest as it acts as a flow and thermal barrier between the upper (less saline) and lower

128 (more saline) Lacq reservoirs (Bahnan et al., 2020). The SSM contains a smaller quantity of

129 clay minerals, which are mostly non-swelling in nature (predominantly illite-rich). Expulsion

130 of water from the compaction of the clay-rich SSM could have contributed to dilution of the

131 aquifer water in the upper Lacq reservoir according to Bahnan et al. (2020).

132

133 **2. MATERIALS AND METHODS**

134 2.1 Starting materials

135 The two materials selected for this experiment were MX80 smectite clay (450 g, MX80

136 experiment) and powdered Sainte-Suzanne marl (550 g, SSM experiment) from the Aquitaine

137 basin (borehole LA 101; latitude 43.420648° and longitude -0.619980°). MX80 is well

138 characterized and widely studied in numerous compaction studies (Sauzéat et al., 2001;

139 Neaman et al., 2003; Mondol et al., 2007; Karnland et al., 2007). It consists of 75 wt% Na-Ca

140 montmorillonite, 15 wt% quartz, 5-8 wt% feldspars (plagioclase and microcline) with lesser

141 amounts of kaolinite, phlogopite, calcite, siderite, pyrite and organic carbon (Bradbury and

142 Baeyens, 2003). In contrast, the clay component of the SSM, as characterized with SEM and

143 XRD, consists of 61 wt% illite, 16 wt% quartz, 10 wt% feldspars (anorthite and albite), 7 wt%

144 kaolinite, 3.5 wt% calcite, while the remainder of the rock comprising cristobalite and pyrite.

145 In terms of the particle size of the materials, approximately 80% < 63 µm for MX80 and

146 around 90% < 63 µm for SSM. Due to the high smectite content, the MX80 has a brut cation

147 exchange capacity (CEC) of 70 meq/100g while the brut CEC for SSM is 9.8 meq/100g.

148

149   2.2 Experimental setup

150   In this study, two long-term experiments using two distinctly different clay-rich materials

151   were carried out at GeoRessources laboratory, Vandoeuvre-lès-Nancy, France. A high

152   stress/fluid pressure/temperature oedometric type cell was designed to experimentally

153   simulate the diagenetic processes (fluid and heat flow, mechanical and chemical compaction)

154   involved in the production of formation water from a saturated clay sample under deep burial

155   conditions (around 6 - 7 km deep). Oedometric tests simulate the one-dimensional (vertical)

156   deformation and drainage conditions: no lateral displacement of the cylindrical sample is

157   possible, but the sample can swell/compress vertically in response to changes in axial

158   (vertical) stress σ_1. For this experiment an oedometric cell, with internal dimensions of 10 cm

159   diameter and 10 cm height, is connected to a set of pressure pumps for generating both pore

160   fluid pressure (Pi) at both sample sides to allow drainage conditions, and a vertical stress up

161   to 45 MPa and 150 MPa respectively, which can be individually controlled to induce the

162   desired effective vertical stress to the sample (σ_1'= σ_1- P_i). Fig. 1 shows the experimental

163   setup for the study: the oedometric cell [A], the oil-pressure generator (for the axial stress)

164   [B], the fluid circulation system [C], the control and data acquisition systems [D], the system

165   for heating control [E]. The oedometric cell is encased by two thermal heating rings to

166   regulate the temperature up to 150°C. An inlet/outlet for fluid from the pore pressure

167   generator pumps are positioned at both the top and bottom of the cell. Two 3 mm thick porous

168   plates (retaining 98% of particles > 16µm) sit on opposite sides of the sample. The fluid can

169   therefore uniformly percolate into/out of the sample. Because of valves placed between the

170   pressure generator pumps and the inlet/outlet of the cell, flow can occur in both directions.

171   The pore pressure generator pumps [C1 & C2], each with a capacity of 100 mL, can apply a

172   constant fluid flow (0.00001–30 ml/min) or a constant fluid pressure. The data acquisition

173   system allows for recording both the axial stress (σ_1) and the pore fluid pressure (P_i). Axial

7

174 deformation is recorded from an externally fitted linear variable differential transformer

175 (LVDT) sensor. The volumes of fluids in both of the pore pressure pumps are also

176 continuously recorded thus allowing the calculation of the water and chemical mass balance
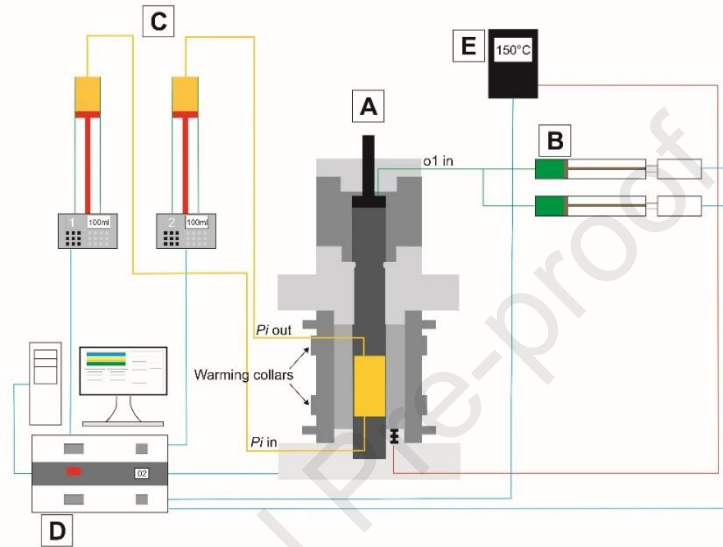
177 of the system.

178

179
180 *Figure 1: Illustration of the experimental system showing the compaction (oedometric) cell*
181 *[A] and various operation systems: the oil-pressure generator (for the axial stress) [B], the*
182 *fluid circulation system [C], the control and data acquisition systems [D], the system for*
183 *heating control [E].*
184

185 2.3 Experimental protocol

186 The compaction protocol followed a series of axial stress and temperature steps for up to 200

187 days. This study was not attempting to reproduce a specific basin or reservoir, therefore

188 common values for axial load and thermal gradients and a constant pore pressure were

189 selected. For the duration of the experiment the pore pressure was maintained at 45 MPa

190 while the axial stress was increased from 45.5 MPa to 150 MPa (maximal effective stress: 105

191 MPa) by increments of ~ 25 MPa. Temperature was increased from room temperature to 150

192 °C by increments of 30°C.

193   Filtered natural Atlantic Ocean water (0.1 µm) sampled of the coast of Bidart (France), was

194   used for both experiments. The chemical composition of the ocean water is given in Table 1.

195   The experimental conditions were progressively applied in the following order:

196   1. Application of a low axial stress ($\sigma 1 = 1.5$ MPa) for the sample saturation;

197   2. Hydration of the dry powdered material in the cell from both the top and bottom inlet

198   at low injection pressure of ~1 MPa;

199   3. When the clay was fully hydrated (i.e. no more fluid was taken up by the clay

200   material), a pressure gradient was applied (from the bottom to the top) until the bottom

201   injection pump C1 was emptied, thus allowing water flow and complete chemical

202   equilibration. At the end of this step, the injection pump at the bottom C1 was isolated

203   from the oedometric cell with a valve, so that no new water will be injected during

204   compaction. The injection pump at the top C2 was almost entirely emptied; only a

205   small amount ocean water was kept to maintain pore pressure in the sample and to

206   collect the expelled water during the experiment.

207   4. Application of the vertical stress ($\sigma 1 = 45.5$ MPa) using a loading rate of 0.001 MPa/s;

208   5. Application of the interstitial pressure (Pi = 45 MPa) using a loading rate of 0.002

209   MPa/s;

210   6. Beginning of the stepwise incremental increase of the vertical stress ($\sigma 1$ max =

211   150MPa) using a loading rate of 0.001 MPa/s and simultaneous application of

212   incremental temperature increase.

213

214   The duration of the steps varied between two and four weeks to allow for the stabilization of

215   the axial compaction (deformation) curves.

216   Expelled fluid was sampled as soon as the minimum required volume of 2 ml has

217   accumulated in the collection pump C2. Fluid was not expelled at each step. The last

218   sampling was done at step 3 (105 MPa, 90°C) for SSM and at step 4 (125 MPa, 120°C) for

219   MX80.

220

221   2.4 Analytical methods

222   Chemical and isotopic analyses of fluids

223   To measure variations in the fluid composition over time, expelled fluid was sampled for each

224   stress step. Upon collection;

225   1.   the pH was measured;

226   2.   the sample was filtered (0.025 µm) to remove any suspended clay particles, and

227   3.   split into two aliquots.

228   A proportion was diluted and acidified (2% HNO_3) for ICP-MS analysis and the remainder

229   was refrigerated in an airtight flask for later isotope analyses. Elemental concentrations were

230   assessed using an Agilent 7900 quadrupole ICP-MS at the Institut du Globe de Physique de

231   Paris (IPGP), France and Cl isotope analyses were carried according to Kaufmann et al.

232   (1984); Eggenkamp (1994, 2014b) and Godon et al. (2004). Repeated analysis of Atlantique 2

233   seawater reference (Godon et al., 2004) gave $\delta^{37}Cl$ reproducibility of $\pm$ 0.03‰ (1σ, n = 48).

234   For the extraction and measurement of Br isotopic content, the protocol thoroughly described

235   by Eggenkamp and Louvat (2018) was closely followed. Br is extracted by distillation in the

236   presence of nitric acid and trapping it in an ammonia solution. The distillation method has

237   been shown to be an effective alternative to the customary extraction by ion exchange

238   chromatography on anion exchange resin (Louvat et al. (2016)) in cases where high Cl

239   content can be problematic to Br extraction due to supersaturation of the resin by Cl. A dilute

240   nitric acid solution will oxidize Br^- to Br_2 but will not oxidize Cl^- therefore a solution

241   containing little to no Cl^- can be produced from solutions with large Cl/Br ratios, by the acid

242   distillation method. Trapping the solution in a strongly reducing alkaline environment such as

10

243   an ammonia solution disproportionates the Br_2 to Br^- and BrO_3^- in a ratio of 5:1. Due to the

244   reducing nature of the ammonia solution the BrO_3^- is then reduced to Br^-. Enough sample

245   should be used to provide a minimum of 20 μg Br. For ocean water, the distillation requires

246   that 1 ml HNO_3 (69%) is added to ~ 0.5 ml sample plus 3.5 ml de-ionized water, immediately

247   closed up and vigorously boiled over a low heat source for 8-10 minutes until the 1 ml of 0.5

248   M NH_3 on the trapping end of the distillation has doubled in volume - i.e. 1 ml has been

249   distilled. This solution is then analyzed with a Thermo Neptune multi collector inductively

250   coupled plasma mass spectrometer. An average of 5 repeated measurements was used to

251   calculate the $\delta^{81}Br$, giving a reproducibility of ±0.11‰ (2σ, n = 60).
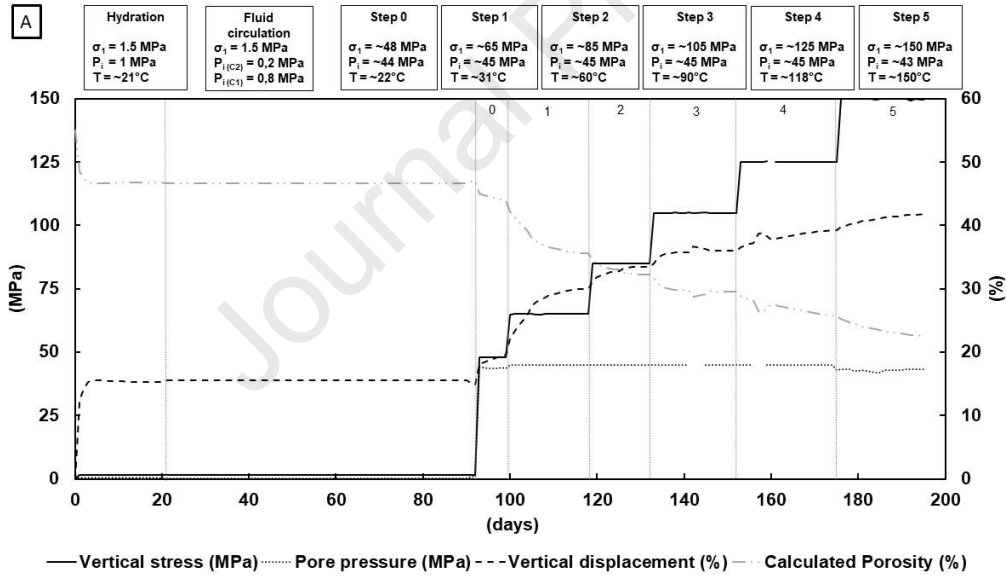
252   After completion of the experiments, the compositions of the two compacted cores were

253   characterized by semi–quantitative X-ray diffractometry (XRD) at GeoRessources laboratory.

254   XRD patterns were collected on a D8 Advance Bruker AXS diffractometer at 35 kV and 45

255   mA with non-monochromatic CoKα radiation (λ = 0.17903 nm), with an iron filter to

256   suppress the Kβ emission, and equipped with a LynxEye fast linear detector. Intensities were

257   recorded from 3 to 75°2θ with a 0.035°2θ step using a 3s counting time per step. For the fine

258   clay fraction (< 2 microns), intensities were recorded from 2 to 40°2θ with a 0.02°2θ step

259   using a 4s counting time per step. Data reduction and analysis were performed with the EVA

260   software (DIFFRACplus from Bruker) and diffraction peaks were identified by comparison

261   with powder diffraction files (PDF2 database from the International Center for Diffraction

262   Data, ICDD).

263

264   **3. RESULTS**

265   3.1 Physical parameters

266   Figure 2 represents compaction curves for the two experiments (the convention of positive

267   compressions for stress and displacement is used) and Table 1S (Supplementary Material)

shows the volumes of water that were collected during the two experiments. During the

hydration and equilibration step, the vertical stress was equal to 1.5 MPa to compensate the

swelling pressure of the MX80 due to the strongly adsorbed interlayer water, which means

that no swelling (dilatant deformation) could be observed. On the contrary, compaction was

observed. In the absence of swelling clay minerals, the SSM compacted more (25%) than the

MX80 (15%). This is due to the swelling pressure maintained by the MX80. Both materials

absorbed similar volumes of water (about 100 mL) and for both the materials the largest

volumes of water were expelled during the earlier compaction steps. Water was not expelled

at each step. At the end of experiment 30% of the initial volume of absorbed water was

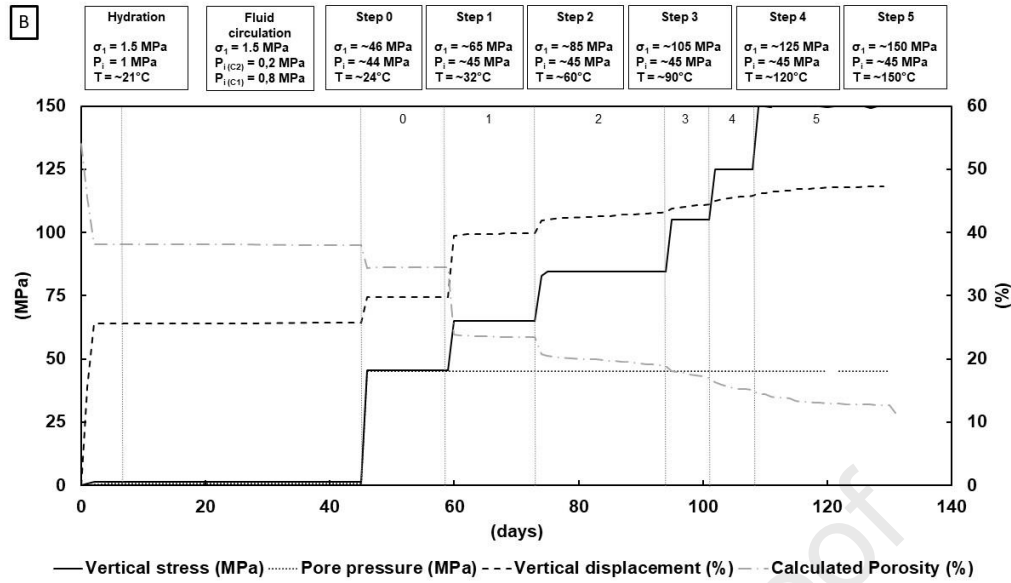expelled for the MX80 experiment and 52% for the SSM experiment.

	Hydration	Fluid circulation	Step 0	Step 1	Step 2	Step 3	Step 4	Step 5
A	σ_1 = 1.5 MPa P_i = 1 MPa T = ~21°C	σ_1 = 1.5 MPa $P_{i(C2)}$ = 0,2 MPa $P_{i(C1)}$ = 0,8 MPa	σ_1 = ~48 MPa P_i = ~44 MPa T = ~22°C	σ_1 = ~65 MPa P_i = ~45 MPa T = ~31°C	σ_1 = ~85 MPa P_i = ~45 MPa T = ~60°C	σ_1 = ~105 MPa P_i = ~45 MPa T = ~90°C	σ_1 = ~125 MPa P_i = ~45 MPa T = ~118°C	σ_1 = ~150 MPa P_i = ~43 MPa T = ~150°C

——Vertical stress (MPa) ········ Pore pressure (MPa) - - -Vertical displacement (%) —·— Calculated Porosity (%)

280

281 *Figure 2: Compaction curve as a function of time for MX80 (A) and SSM (B). The same*
282 *vertical stress, pressure and temperature increments were followed in both experiments. The*
283 *pore pressure was maintained at 45 MPa while the vertical stress was increased from 45.5*
284 *MPa to 150 MPa by increments of ~ 25 MPa. Temperature was increased by increments of*
285 *30°C from step 1.*
286

287 The compaction leads to a variation of the sample porosity which cannot be measured during

288 the experiment but only estimated from the bulk volume variations of the system. The

289 decrease in total porosity, calculated from the volumetric mass densities, occurs mainly

290 during the step at 65 MPa and 30°C. At the end of experiment the porosity drops from 55% to

291 22% for MX80 and from 54% to 16% for SSM. Mercury porosity measurements performed

292 after experiments give 8% of free porosity and 9% of trapped porosity for a total of 17% of

293 connected porosity for MX80. The values are 4.4%, 3.6% and 8% respectively for SSM. This

294 means, a large proportion (53% for MX80 and 45% for SSM) of the porosity is trapped (i.e.

295 pores no longer have a continuous path towards the sample surface). Intrusion of mercury into

296 a cavity is controlled by the size of the pore throat radius while the radius of the cavity and its

297 connectivity controls extrusion of mercury from the cavity. The median pore diameter is 7 nm

298 for MX80 and 9 nm for SSM. The discrepancy between the mercury porosity and calculated

299 porosity can be attributed to the absorbed water content present in the clay.

300   The CEC slightly increases for MX80 to reach 77 mEq.100g^{-1} (70 mEq.100g^{-1}initially) and

301   doesn't change for SSM and stays at 9.8 mEq.100g^{-1} after experiment. This could be due to

302   the slight mineralogical changes observed during MX80 compaction.

303

304   3.2 Mineralogy

305   X-ray diffractograms are shown in Figure 3 and 4. Some modifications of the global

306   mineralogical composition of solids has been observed after both experiments. For MX80, the

307   main transformation concerns the montmorillonite. Its interlayer composition changes after

308   experiment characterized by an enrichment in Na and K (shift of the (001) peak toward higher

309   2θ angles). Ca is expelled from the crystallographic structure. A possible but limited

310   illitization could be envisaged. Phlogopite is likely altered if considering that the amount of

311   quartz and calcite has not changed during experiment (based on the comparison of the

312   intensities of their peaks). Plagioclases crystallize (albite and anorthite). Peaks of gypsum are

313   not observed on the diffractogram after experiment, it probably dissolves. Two peaks around

314   51.5 °2θ and 62.6°2θ were difficult to attribute to the phases already identified. They could

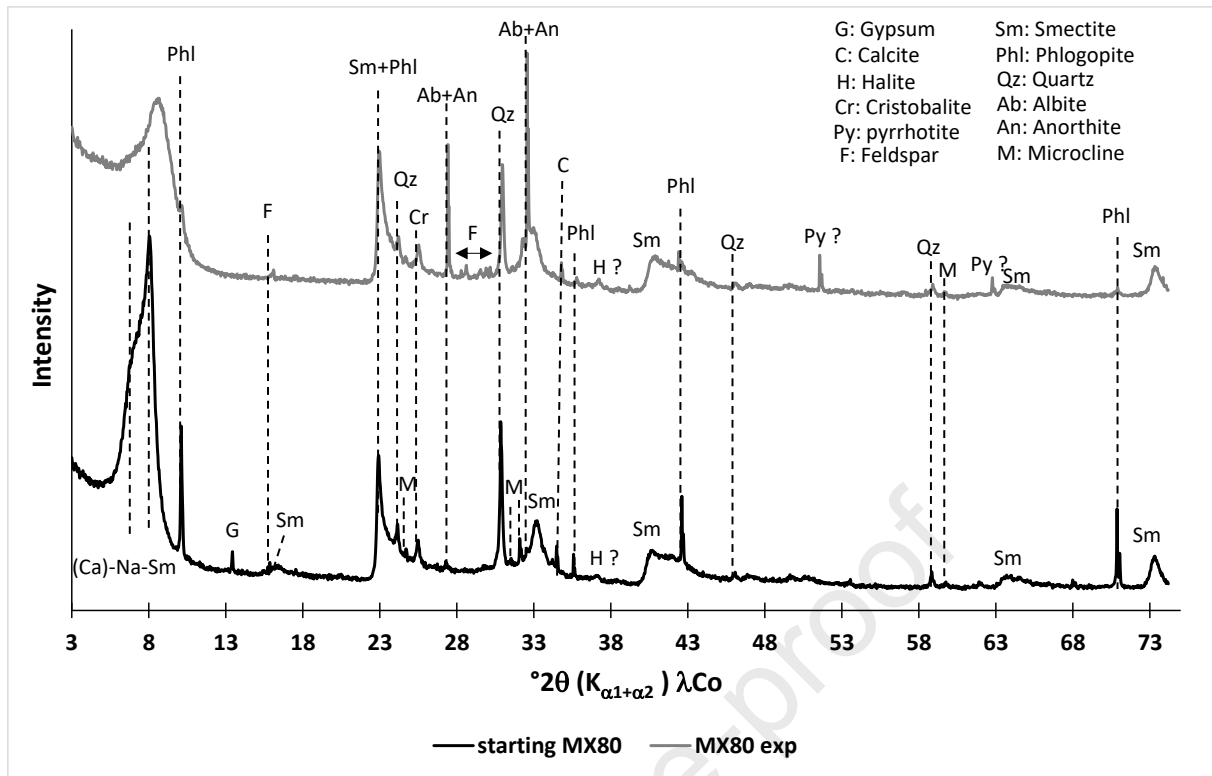315   match with pyrrhotite.

316

Figure 3: X-Ray diffractograms of the MX80 sample before and after experiment (starting MX80 and MX80 exp respectively).

For SSM, assuming that the quartz is not affected during the experiment (intensity of the main quartz peak identical on the two diffractograms of figure 4), a significant decrease in the intensity of kaolinite, illite and anorthite peaks can be attributed to a drop in the amounts of these three minerals during experiment. The most altered mineral would be kaolinite. Low intensity peaks of chlorite appear on the diffractogram of the sample after experiment. Calcite and pyrite seem unaffected. It has to be noticed that it is not possible to determine the moment when the mineralogical transformation occur during experiment. It can be envisaged that the main transformations happen at higher temperatures thus rather at the end of experiment, because kinetics are more favorable.

15

331

332
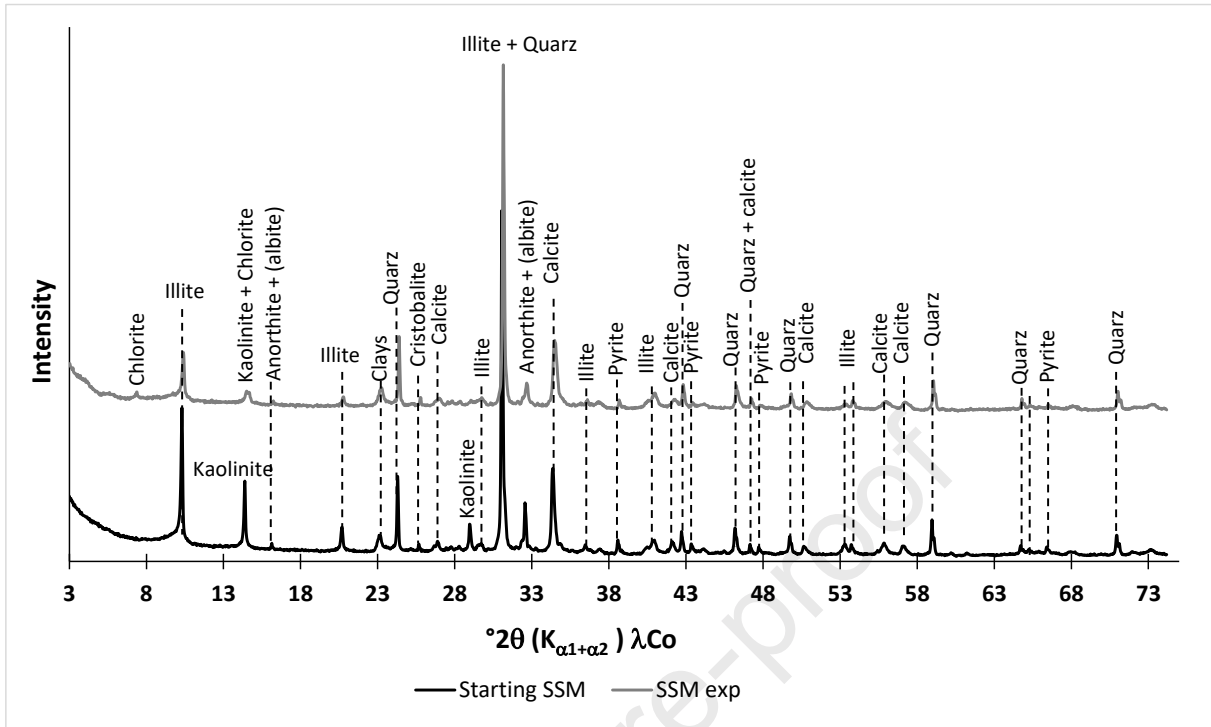
Figure 4: X-Ray diffractograms of the SSM sample before and after experiment (starting SSM and SSM exp respectively).

333
334

335
336

337   3.3 Fluid chemistry

338   Table 1S (Supplementary Material) shows the volumes of water that were collected during the

339   various compaction steps. 96.3 ml of ocean water were absorbed and only 28.9 ml of water

340   (30%) were expelled during the compaction experiment for MX80 experiment. For SSM

341   experiment, the absorbed volume was 107.5 ml but more than 52% (56.3 ml) was expelled.

342   During compaction step 1, two separate samples were collected in the 14-15 days at the same

343   pressure and temperature. For the next steps, the volume collected were significantly lower

344   and some steps didn't expel any water.

345   For the MX80 experiment, the ocean water is first cycled through the clay under a minimum

346   load of 1.5 MPa to reach the best close to equilibrium state between the clay and ocean water.

347   The resulting water is called "initial water" in (Table 1). The initial water is significantly

348   different from the Bidart water: the Cl, Br and Na concentrations increase by around 10%.

16

349   Interestingly, this is not the case for K. A more pronounced enrichment is observed for Ca and

350   S maybe due to fast equilibrium with sulfate and carbonate minerals. Si, and Mg are less

351   concentrated in this initial water. The first step of compression to 45 MPa leads to the more

352   pronounced variations of the water chemistry. The concentrations of Na, K, Mg, Ca, Cl, Br

353   and S increase by 35 to 40% by comparison with the Bidard composition. Then, the following

354   steps of T and P increase roughly lead to a progressive decrease of the concentrations of Na,

355   K, Mg, Cl and Br in the expelled solution. At the end of experiment, the salinity expressed by

356   the ionic strength I of the expelled solution has dropped from 0.7 to 0.37. The pH of the initial

357   solution is 8.1 and we can observe a slight drop of the pH during experiments with values

358   ranging between 7.7 and 8.0.

359   Concerning the SSM experiment, the results are quite different. The initial water assumed to

360   be in equilibrium with the marl, shows increasing concentrations for Ca, S and in to a lesser

361   extent K, likely to be attributed to chemical equilibrium with carbonate and sulfate minerals

362   for calcium and sulfur. The steps of increasing P and T lead to slight variations of the solution

363   chemistry. Notice that the last solution was collected at 105 MPa and 90°C. No more water

364   was expelled during the last two steps. The pH of the solution slightly decreases from 8.2 to

365   7.6 during the different steps of the experiment.

366

367

Table 1 : Chemical composition of the aqueous solution sampled in the MX80 and SSM
experiments. I is for ionic strength calculated from major elements. Concentrations in
mmol.L⁻¹.

	Sample description	I	pH	Na	K	Ca	Mg	Si	S	Cl	Br
	Bidart	0.697	8.1	481.9	10.1	10.7	54.6	1.16	24.7	524.1	0.88
MX80	Initial pore water*	0.746	7.7	538.2	8.43	17.73	42.74	0.41	31.9	570.7	0.97
	45.5 MPa	0.948	7.8	649.5	13.90	14.28	75.27	0.28	33.1	738.6	1.24
	65 MPa & 30°C	0.728	7.7	548.6	6.48	20.36	27.92	0.96	48.9	497.7	0.81
	65 MPa & 30°C	0.754	7.7	576.1	5.49	21.67	24.73	1.04	52.5	514.6	0.83
	85 MPa & 60°C	0.653	7.9	501.4	4.48	17.88	20.34	1.26	47.7	436.2	0.71
	125 MPa & 120°C	0.370	8.0	296.5	2.38	8.31	9.36	2.45	23.6	238.1	0.38
SSM	Initial pore water*	0.710	8.2	497.2	12.3	25.9	37.3	0.33	36.3	506.4	0.78
	65 MPa & 30°C	0.705	8.1	488.7	11.4	25.5	39.2	0.46	35.2	503.1	0.77
	65 MPa & 30°C	0.726	7.9	507.2	11.7	25.3	40.8	0.40	35.4	520.6	0.80
	85 MPa & 60°c	0.705	7.9	490.4	12.0	25.3	38.7	0.80	33.6	504.3	0.78
	105 MPa &90°C	0.746	7.6	521.1	13.1	25.0	40.5	0.58	36.5	541.2	0.84

*The initial pore fluid concentration refers to the re-equilibrated ocean water composition,
i.e. the composition of the ocean water after it has circulated through the clay before the
compaction.

374

3.4 Cl and Br concentrations and isotopes

The evolution of both concentrations and isotopes ratios for Cl and Br are given in Fig. 5 for

the MX80 and SSM experiments. Fig 6 shows that Cl and Br concentrations are correlated.

The range of variations is however more marked in the MX80 experiment than in the SSM

experiment. The $\delta^{37}Cl$ value of the initial Bidart ocean water is -0.12‰ (±0.03) and the Cl

content is 524 mmol.L⁻¹. After equilibration with MX-80 the first notable Cl isotope variation

occurred.

382

The $\delta^{37}Cl$ of the re-equilibrated ocean water has decreased to -0.2‰ (±0.03). With

pressurization to 45 MPa, $\delta^{37}Cl$ values reach 0.02‰ (±0.02) in the first water expelled with a

significant enrichment in Cl (738 mmol.L⁻¹). The $\delta^{37}Cl$ values then decreased with increasing

pressure and temperature, together with the Cl concentration. The variation that occurs at 65

MPa (step 1) is noteworthy. As mentioned before, two samples were collected during this

18

step. In the first water expelled at 65 MPa, the $\delta^{37}Cl$ was -0.24‰ (±0.03). After 14 days at the

same pressure and temperature conditions, the $\delta^{37}Cl$ value has decreased to -0.45‰ (±0.03),

but keeping a comparable Cl concentration. Following the variation at 65 MPa and 30°C, no

more significant fractionation occurred in the water expelled from the MX-80 compaction,

but the last step is characterized by the lower Cl content (238 mmol.L^{-1}).

The SSM experiment show very weak variations of both Cl content and $\delta^{37}Cl$.
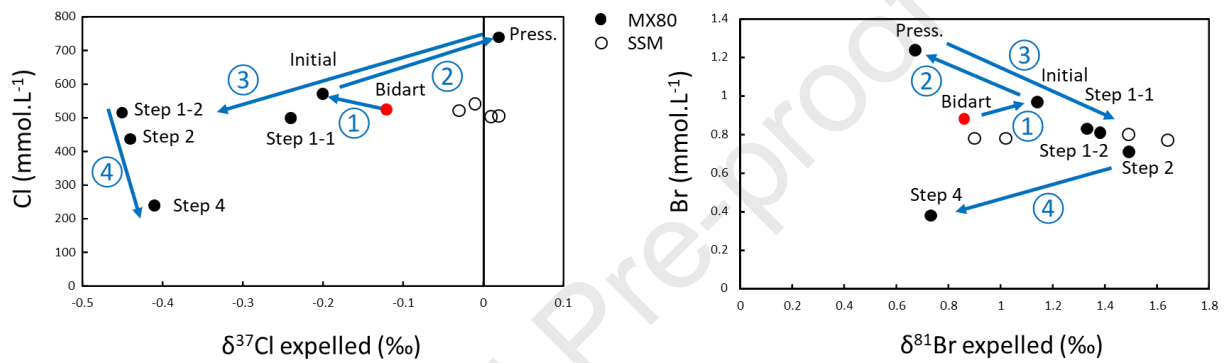

Fig. 5: Concentrations and isotope compositions of Cl and Br in the MX80 and SSM

experiments. The different steps of compaction are given for MX80. "Press." means pore

pressurization at 45 MPa. "Bidart" corresponds to ocean water sampled at Bidart (France).

"Initial" corresponds to the values of equilibrated water before the beginning of compactions

steps. The blue arrows correspond to the different successive mechanisms described in the

discussion.

Regarding Br isotopes, two important observations can be seen from Fig. 5. Firstly, the range

of Br variation observed, is larger than the range of variation of Cl and secondly, $\delta^{37}Cl$ values

are negatively correlated with the $\delta^{81}Br$. The initial Bidart ocean water has a $\delta^{81}Br$ value of

0.86‰ (±0.07).

A delta value of 0.86‰ is highly unlikely for ocean water (Eggenkamp et al. (2019)).

Preliminary data obtained from halite samples suggested that the values for the Br isotopes

19

409   should not be higher than 0.5‰, the value of the reference standard from the IPGP. A

410   possible bad distillation may have happened, but seems unlikely as to increase the value by

411   0.86‰ is so large that something very strange must have occurred during distillation that it

412   could not have gone unnoticed. What however may be possible is that the high value is

413   related to the sample location, which was along the coast: Br isotopes can change because of

414   interaction with organic material, but the magnitude of fractionation, is not known and has

415   also never been studied in detail. Little attention is given to this problem. The purpose of the

416   study is after all to course the changes in isotope ratios due to compaction, and in principle for

417   that study, the primary isotope ratio of the sample is not important, only the changes that

418   occur during the experiments.

419   After the equilibration with MX80, the first significant variation was observed as the δ^{81}Br of

420   the initial water reached 1.14‰ (±0.01). With pressurization to 45 MPa the δ^{81}Br decreases to

421   0.67‰ (±0.12). The significant variation of Cl isotopes that is observed for the two samples

422   collected during the step at 65 MPa & 30°C, is not seen for Br. The δ^{81}Br value for the first

423   sample at these conditions was 1.38‰ (±0.05) and for the next, 14 days later, was 1.33‰.

424   (±0.14). When compaction of the MX-80 progresses, the δ^{81}Br values continue to increase up

425   to 1.5‰ (±0.01) at 85 MPa & 60°C before it decreases to 0.7‰ (±0.22) in the water expelled

426   at 125 MPa & 120°C.

427   During SSM compaction the range of Br isotope variation that occurs shows a similar range

428   as observed during MX-80 compaction (Fig. 5). In comparison, during the SSM compaction,

429   the δ^{81}Br value changes from 0.86‰ (±0.07) in the Bidart ocean water to 1.02‰ (±0.12) after

430   it has been re-equilibrated with the clay (initial pore water). A significant shift to 1.6 ‰

431   (±0.12) is observed in the water expelled at 65 MPa and 30°C. In the second sample collected

432   at the same pressure and temperature conditions, 14 days later, the δ^{81}Br is 1.5‰ (±0.12). At

433   85 MP and 90°C, the $\delta^{81}Br$ value decreases suddenly to 0.9‰ (±0.07) before the value

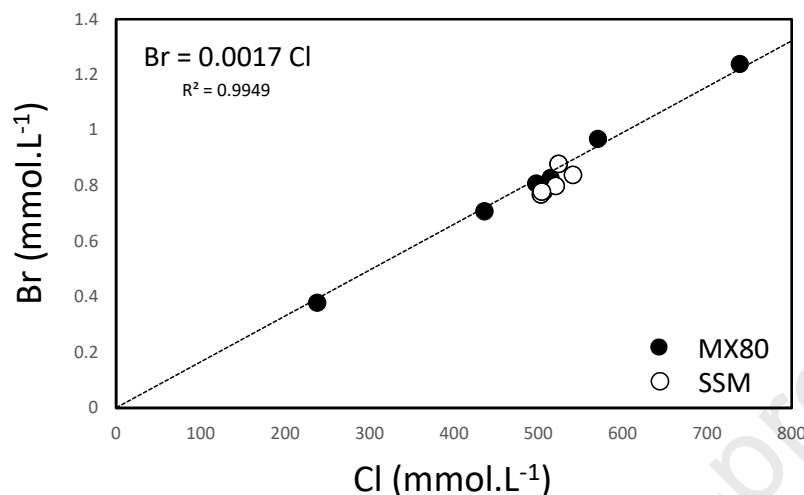434   increases to 1.5‰ (±0.10) in the last expelled water collected.

435

436

437   Fig. 6. Br and Cl concentrations in the expelled fluid of MX80 and SSM experiments.

438

439   **4. DISCUSSION**

440

441   To interpret the results of the compaction experiments, we have to decipher the different

442   mechanisms that are responsible for the chemical and mineralogical evolution of the system.

443   XRD analyses show that the mineralogical transformations remain limited. The main

444   transformation concerns the MX80 experiment with a part (10 to 15%) of the smectite being

445   transformed in sodic montmorillonite, kaolinite and albite. In the SSM experiment,

446   experimental data predict a weaker reactivity of the system. This is well confirmed by the

447   chemistry of the expelled water that remains roughly constant whatever the experimental

448   conditions applied.

449   Thus, assuming limited mineralogical transformations in terms of dissolution/precipitation

450   processes, the evolution of the chemistry of the solution is a result of either

451   adsorption/repulsion on the negatively charged surface of clay minerals and/or elements

21

452   trapping due to the decrease of clay porosity under compaction. This is especially applicable

453   for elements such as halogens that are poorly incorporated in secondary minerals that could

454   precipitate during the compaction.

455   Another important point is that the expelled volume is small by comparison with the

456   remaining water (several percent at each step). Consequently, to better understand the

457   behavior of elements, a mass balance has to be calculated to evaluate the bulk chemical

458   composition of the pore water. Table 1S (Supplementary Material) presents the concentrations

459   of halogens both in the expelled water and that calculated in the pore water. Notice that the

460   mass balance is not performed for cations since they are more sensible to chemical reactions

461   despite limited. When looking at the variations of Cl and Br concentration in the pore water,

462   they remain very very low by comparison with that of the expelled water. That is to say that

463   the chemical equilibrium between expelled water and pore water is never achieved in the

464   experiment.

465   To understand the chemical and isotopic evolution of the system, a special attention has to be

466   paid to the different types of pore water in clays, to the anion exclusion effect and to the

467   evolution of the porosity with compaction leading to a change of the dominated transport of

468   solute.

469

470   4.1 The diffuse double layer (DDL)

471   Clay minerals are characterized by their stacking of tetrahedral (T) and octahedral (O) sheets

472   forming layers. The isomorphic substitution of cations in sheets (Si^{4+}-Al^{3+} substitutions in

473   tetrahedron or Al^{3+}-Mg^{2+} substitutions in octahedron for instance) is responsible for

474   permanent negative surface charge of clay minerals (Brigatti et al., 2013). The negative

475   surface charge causes individual layers to accumulate in stacks and stacks to arrange in edge

476   to edge or edge to face structures. This arrangement creates interlayer and interparticle spaces

22

477 which can be filled by water. As a consequence of the surface charge, the whole water trapped

478 in the clay porosity does not respect the electrical neutrality, especially in the vicinity of the

479 clay surface (Revil and Leroy, 2004) where hydrated counterions (cations) are sorbed directly

480 onto the negative particle surface mainly due to electrostatic interactions (Langmuir, 1918;

481 Stern, 1924). In the diffuse layer, ions are more loosely attracted to the surface via Coulomb

482 forces and can move in the fluid under the influence of electric attraction, thermal motion or

483 concentration gradients.

484 So the interparticle layer is composed of the DDL and the free pore water. The concentration

485 of counter-ions decreases with distance from the charged particle surface until there will be no

486 distinction between the DDL and the free pore water. Smaller cations are prominent in

487 interlayer and bound water while large anions dominate the free water fraction in the

488 interparticle space. Anions with the greatest polarization potential (ability of an anion to be

489 distorted by a cation) are preferentially adsorbed. This is usually the largest anions. The

490 adsorbed ions are also governed by the composition and the ionic strength of the solution

491 surrounding the particle (Brady and Weil, 2008). Cl and Br form sufficiently strong

492 associations with cations to occur as neutral or positively charged ion pairs or clusters in the

493 DDL (Neuzil and Person, 2017). According to Celejewski et al. (2018) chlorine can be

494 included in the diffuse layer (bound water) while bromine will remain in the free water

495 fraction as Cl preferentially associates with cations compared to Br (Eggenkamp and

496 Coleman, 2009). Therefore, another consequence of the negative surface charge of clays

497 concerns the transport of anions in the different porosities: because the anions are repulsed by

498 negatively charged mineral surfaces, only a part of the total porosity is accessible for anions
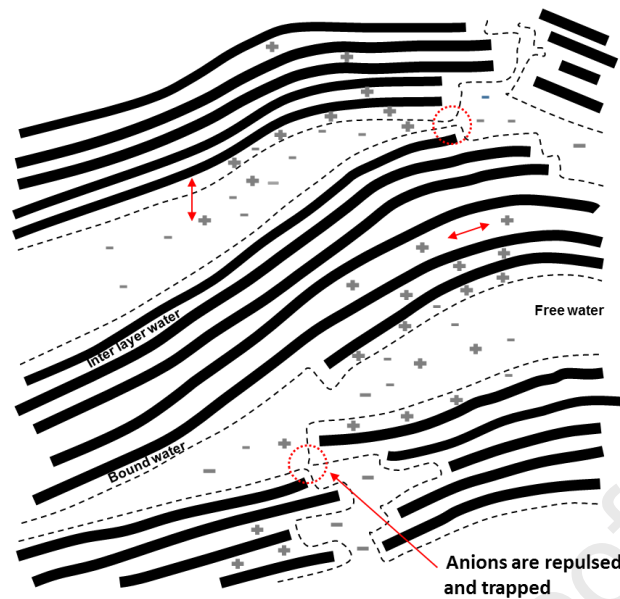
499 transport.

23

500

501　*Figure 7: An illustration of the influence of the negative charge of clay particles on the*

502　*physical and chemical morphology of clay rock pore spaces showing progressive expulsion*

503　*and trapping and of the Cl and Br anions during compaction of negatively charged stacks.*

504　*Red arrows represent the possible motions of ions in interlayer water and between free water*

505　*and bound water.*

506

507　4.2 Anion exclusion during clay compaction

508　During compaction of clays, the interparticle porosity will decrease first while the interlayer

509　porosity will remain more or less constant (Muurinen et al., 2004). With increasing

510　compaction, the interlayer porosity will also start to decrease (found to occur at bulk dry

511　density >1300 kg/m^3, Van Loon et al., 2007). Due to the very narrow spaces created between

512　clay particles within clay mineral stacks, the double layers in the interparticle porosity

513　approach one another until they finally overlap. As a result, the negative electric potential in

514　the interlayer space increases and all anions will be expelled from the interparticle porosity

515　(Bolt and de Haan, 1982; Pusch et al., 1990; Wersin et al., 2004, Wigger and Van Loon,

516　2017). The resulting interparticle water now contains only cations while anions dominate the

24

517   largest remaining interparticle porosity. At high compaction rates, the porosity mainly

518   consists in interlayer porosity (Bourg et al., 2006), the interparticle porosity having almost

519   entirely disappeared.

520   This phenomenon leading to the expulsion of anions of the decreasing porosity referred to as

521   'the anion exclusion effect'. In the case of high ionic strength of the pore solution, the

522   majority of experimental or modeling studies show that the accessible porosity for anions

523   increases. This is mainly explained by the fact that the volume of the DDL decreases due the

524   high concentration of counterions in the solution able to counterbalance the mineral surface

525   charge (Plecis et al., 2005). In addition to anion exclusion, overlapping DDL's also creates a

526   charge barrier or blockage between converging clay particle stacks (Appelo et al., 2010). This

527   prevents the passage of anions in free water. Therefore anions can either be trapped inside the

528   diminishing pore spaces, and this is a function of the ion size, or forced to travel via longer

529   transport routes through the clay layer, retarding transport, as illustrated in Fig.7. This is

530   referred to as tortuosity (Melkior et al, 2009),

531

532   4.3 Transport in compacted clays

533   In fine-grained low-porosity clayey aquitards, where advective flow is low or absent,

534   diffusion becomes the dominant transport mechanism. In clayey materials, the excess charge

535   of clay minerals counterbalanced by ions of opposite charge induces electrostatic interactions

536   that influence the mobility of ions in the solution. The mobility of ions is a function of the

537   salinity and thus the ionic strength of the solution, its viscosity, the water content, the

538   electrical charge of the clay surface, the temperature by the effect of Brownian movements,

539   the pressure, the size and charge of the considered ions, the pore size of the medium and its

540   tortuosity.

541   Electrostatic interactions increase with the salinity or the ionic strength of the solution

542   resulting in slower diffusion of ions. The diffusion kinetics decreases when solution

543   concentration increases (Schauble et al., 2003). Results from other diffusion experiments with

544   clay-rich materials have shown that cation diffusion is normally enhanced compared to anion

545   diffusion due to interlayer and DDL diffusion (Shackelford and Daniel, 1991; Sato et al.,

546   1992; Kozaki et al., 1998; Molera and Eriksen, 2002; Van Loon et al., 2004; Van Loon et al.,

547   2007, Descostes et al., 2008).

548   Temperature changes influence the rate of diffusion. Heat causes atoms to vibrate and

549   vibration increases with increasing temperature. Therefore, increasing temperature will result

550   in an enhanced diffusion coefficient (Desaulniers et al., 1986; Eggenkamp et al., 1994;

551   Hendry et al., 2000; Hesse et al., 2006; Luo et al., 2014; Bernachot et al., 2017).

552

553   4.4 Isotope fractionation

554   Theoretically, due to the differences in masses, the different stable isotopes of an element

555   would fractionate during the process of diffusion (Lindemann, 1921). Isotopic fractionation is

556   defined as the relative partitioning of the heavier and lighter isotopes between two coexisting

557   phases in a natural system, i.e. fractionation is a function of the relative difference of masses

558   of the different isotopes. Fractionation is driven either by the equilibrium or kinetics of a

559   system.

560   Therefore, the nature of the chemical bonds (Nygård et al., 2004) and the temperature (Urey,

561   1947) can influence isotopic fractionation. Fractionation normally decreases with increasing

562   temperature (Richet et al., 1977; Schauble et al., 2003; Balan et al., 2019) and stronger

563   chemical bonds generally preferentially involve the heavier isotope (Schauble, 2004). The

564   fractionation in natural systems, such as in sediments, is dictated more by kinetics rather than

565   equilibrium fractionations (solution and precipitation).

566 In order to assess element and isotopic fractionation during diffusion, there are three things

567 that should be considered separately: (1) the relative atomic masses difference between Cl and

568 Br, (2) the relative masses difference between ^{81}Br and ^{79}Br and (3) the relative mass

569 difference between ^{37}Cl and ^{35}Cl. The Cl anion has a smaller radius than Br at 167 picometer

570 and 182 picometer respectively. However the atomic mass of Br isotopes (78.9 and 80.9

571 g.mol^{-1} for ^{79}Br and ^{81}Br respectively), are more than twice those of Cl isotopes (34.9 and

572 36.9 g.mol^{-1} for ^{37}Cl and ^{35}Cl respectively). Therefore, Br is clearly expected to move slower,

573 so fractionate less, than Cl during diffusion processes (Eggenkamp and Coleman, 2009).

574

575 4.5 Pore Water Evolution

576 The pore water is composed of the interlayer water, the trapped interparticle water, and the

577 free interparticle water. It is this free pore water that is expelled during the experiments.

578 While the DDL is dominated by cations, the Cl and Br anions will mostly be in the free water

579 proportion of the pore water because they are largely excluded from the DDL. As a

580 consequence only a part of the total porosity is accessible for anion transport and the water

581 sampled gives the chemistry of the free pore water. For the MX80 experiment, we see that

582 without any pressure or temperature applied during the hydration phase of the experiments

583 (Arrow 1, Fig. 5), the concentrations of Br and Cl increase, mainly due to the water uptake

584 due to water adsorption by clay minerals. Because there is no movement of the solute during

585 the equilibrium phase and because this phase lasted 90 days, we can expect that diffusion

586 processes could drive the isotopic fractionation observed for both Cl and Br. Diffusion in clay

587 pore waters requires circumnavigating clay particle stacks which considerably increases the

588 distance/length ratio of the pathway (tortuosity) (Melkior et al, 2009). In our experiment, the

589 expelled water contains more of the lighter Cl isotope which is in agreement with the

590 diffusion mechanism. However, because the heavier Br isotope is found in this same water,

591   another mechanism has to be considered, namely possible gravitational fractionation of Br

592   isotopes. Gravitational settlement of heavier Br isotopes. It took a total of 90 days for the

593   completion of the hydration and equilibration (fluid circulation) phase to be completed. Water

594   was sampled at the end of the 90 days. During the fluid circulation phase, water was

595   circulated from the pump connected at the top to the pump connected at the bottom, so that

596   when compaction start, the expelled sample could be collected in the empty pump connected

597   at the top. Therefore, the sample called 'initial water' comes from the pump connected at the

598   bottom of the clay. Gravitational isotopic fractionation is seen in columns of oil and gas

599   reservoirs, in hydrothermal fluids, in sediments and even trapped air (Bons and Gomaz Rivas,

600   2012; Shirdokar et al., 2003; Zang and Kroos, 2001, Guinta et al., 2017). This might also be

601   the case for Br.

602   When compaction started, pore pressure was maintained with the full pump connected to the

603   bottom of the clay, and the expelled samples were collected in the empty pump connected to

604   the top of the clay. This may explain the change in direction of the arrows on Fig 5 from

605   'initial' composition to 'pore pressure' composition. With the first pressurization (Arrow 2,

606   Fig.5), the free pore water is expelled. The dominant mechanism of transport should be

607   advection, so isotopic fractionation due to the pressurization should remain limited. This early

608   compaction corresponds to the most significant decrease in porosity. As we reduced porosity,

609   the composition of the free water, enriched in Cl and Br, can be attributed to the anion

610   exclusion effect. The isotopic composition in Br and Cl is actually the composition enriched

611   in heavier Cl and lighter Br, as a result of the inverse fractionation observed in the hydration

612   step. The largest volumes of water are expelled during early compaction and the composition

613   of the expelled water is supposed to be that of the free water.

614   As compaction continues pore size continues to decrease. The interparticle porosity will

615   decrease first while the interlayer porosity will remain more or less constant (Muurinen et al.,

28

616   2004). When the dry bulk density surpasses 1300 kg.m^{-3} between 45 and 65 MPa, the

617   interlayer porosity will also start to decrease (Van Loon et al., 2007). This further amplifies

618   the anion exclusion and trapping effect. The water expelled is different in composition from

619   the trapped water. Cl and Br concentrations decrease (Arrow 3, Fig. 5) in the water expelled

620   because they are trapped in the porosity by the anion exclusion effect. In addition to being

621   forced to travel via longer transport routes through the clay layer, anions become trapped

622   inside the diminishing pore spaces as a function of the ion size. Diffusion processes are more

623   likely responsible for isotope fractionation implying that lighter isotopes move faster. This is

624   valid for Cl. For Br, it is the heavier (larger) isotope that is preferentially expelled. The

625   efficiency of fractionation is linked to the rate at which an isotope can diffuse away from a

626   repulsive charge (Phillips and Bentley, 1987). ^{35}Cl with higher ionic mobility would be more

627   effectively repulsed by the charge barrier than ^{37}Cl. The heavier ^{37}Cl isotope is also slower to

628   diffuse out of the DDL into the free water when the anions are excluded during increasing

629   compaction (Celejewski et al., 2018) as theoretically, ^{37}Cl isotope associates more strongly

630   with divalent cations which will preferentially remain sorbed (Schauble et al., 2003).

631

632   At the highest compaction steps (Arrow 4, Fig. 5), the effect of higher temperature has to be

633   mentioned because this can lead to faster diffusion and potential mineral transformation. Cl

634   and Br in the expelled water continue to decrease due to diminishing pore size, which can be

635   enhanced by possible mineral precipitation at high temperature. In terms of isotopes the

636   expelled water tends to be slightly enriched in heavier Cl isotope and more significantly

637   enriched in lighter Br isotope.

638   In correspondence to the findings of Kharaka and Berry (1973); Lavastre et al., (2005); Van

639   Loon et al., (2007); and Nakata et al., (2016), the results from this study emphasize that the

640   surface chemistry of the clay is a key factor in the efficiency of the clay to act as a filtration

641   membrane. Smectite rich MX80, with a higher negative surface charge, was a more efficient

642   filtration membrane for both Cl and Br anions compared to the illite-rich SSM, despite the

643   SSM having been compacted to a much lower porosity than the MX80.

644

645   4.6 The case of Br

646   While Cl and Br are not significantly fractionated in the MX-80 experiment, Cl/Br ratio

647   shows small but significant (i.e. beyond analytical uncertainties) fractionation from the early

648   stage to the last step of the experiment compared to the original Bidart ocean water. In this

649   experiment the freshening observed is therefore not only a result of retardation of dissolved

650   solutes (filtration) but rather a result of trapping of the solutes by the clay layer itself. This

651   trapping of the anions within the clay layer is a combination of both physical and chemical

652   interaction between the clay mineral surfaces and the pore fluid.

653   Compaction of MX80 caused isotopic fractionation of Cl and of Br. Larger fractionation was

654   observed for Br. The SSM compaction did not result in fractionation of Cl isotopes. However,

655   compaction of the SSM caused Br isotope fractionation to the same extent as the MX80

656   compaction. This result suggests that Br was more readily fractionated compared to Cl. This

657   result also supports the idea that fractionation is a result of both physical and chemical water-

658   rock interactions, i.e. diminishing porosity and diffusion. However, the range of fractionation

659   achieved during the clay compactions is smaller than what is measured in formation waters

660   (up to - 8‰ for $\delta^{37}Cl$ and 4‰ for $\delta^{81}Br$ (Bagheri et al., 2014), due to the much smaller scale

661   of the compaction experiment.

662   Considering the bromine isotope evolution Kharaka and Berry (1973) found that Br is filtered

663   more effectively by a thin clay membrane compared to Cl due to its higher hydrated ionic

664   potential (a function of charge and radius). The repulsive force created by charge barriers in

665   negatively charged clay under compaction, will therefore generally be stronger on Br than on

666 Cl (and so retardation/preferential expulsion will be more prevalent). In addition, the

667 relatively low concentration of Br compared to Cl (in natural formation waters), any slight

668 uptake or release of Br may significantly affect the bromide concentration (and in effect also

669 the isotopic composition) (Fontes and Matray, 1993; Bozau et al., 2015). What we see here is

670 that it translates into amplified isotope fractionation of Br.

671 For the SSM compaction experiment, despite no change in concentration, Br isotopes were

672 effectively fractionated. Br is the larger ion and has lower mobility compare to both Cl

673 isotopes. The fractionation of Br during compaction might be more sensitive to decreasing

674 porosity than Cl. This notion is supported by the isotopic fractionation for Br observed in the

675 water remaining in the pore pressure generator pump after the SSM compaction (and not in

676 the MX-80 compaction).

677

678 **5. CONCLUSION**

679

680 Our study on the chemical and isotopic fractionation of Cl and Br in water expelled during

681 experimental compaction of clays, showed that they can help to reveal the history of pore

682 fluids in sedimentary basins.

683 Despite showing no significant mineralogical transformations in terms of

684 dissolution/precipitation processes, our experiment showed effective freshening and

685 fractionation of Cl and Br isotopes. The range of freshening and fractionation observed in our

686 experiments is in line with, but smaller than what is measured in natural samples. This is due

687 to the extremely short time of the experiment (compared to geological time) and small volume

688 of expelled water produced during the compaction. In particular, we suggest that:

689   1. Anion and isotope evolution during the compaction of clays is a function of both

690   chemical and physical water-rock interactions. The surface chemistry of the clay in

31

691   combination with decreasing porosity result in re-equilibration of compressed and

692   overlapping diffuse double layers which, in part, drive the anion and isotope

693   evolution.

694 2. The clay with more negative surface charge is more effective in

695   ultrafiltration/freshening of water expelled during compaction irrespective of its

696   degree of compaction.

697 3. Reduction in porosity and the resulting charge barrier created due to overlapping of

698   DDL's causes anions to become trapped in the clay layer. The retention effect is

699   slightly more pronounced for Br than for Cl. This retention can explain the high

700   salinities that are observed in flowback waters produced within the shales after

701   hydraulic fracturing in gas shale exploitations.

702 4. Longer transport routes did not have a significant effect on the concentration of anions

703   in the expelled water but did have a significant effect on the isotope composition due

704   to diffusion processes.

705 5. The range of isotopic fractionation observed for Br is larger than what is seen for Cl.

706 6. The charge barrier resulting from compaction of negatively charged clays caused

707   preferential expulsion of the heavier isotope for Cl and the lighter isotope for Br.

708 7. Fractionation of Cl isotopes is more prevalent during the earlier compaction steps

709   (lower pressures and temperatures). Fractionation of Br isotopes becomes more

710   pronounced at the later compaction steps (higher pressures and temperatures).

711

712 **ACKNOWLEDGEMENTS**

713

723

724 **REFERENCES**

725 Agrinier, P., Destrigneville, C., Giunta, T., Bonifacie, M., Bardoux, G., Andre, J., & Lucazeau,

726 F. (2019). Strong impact of ion filtration on the isotopic composition of chlorine in young

727 clay-rich oceanic sediment pore fluids. *Geochimica et Cosmochimica Acta*, *245*, 525-541.

728 https://doi.org/10.1016/j.gca.2018.11.013

729 Agrinier P., Bonfacie M., Bardoux G., Lucazeau F., Giunta T. and Ader M. (2021) Chlorine

730 isotope data of chlorides challenge the pore fluid paradigm. *Geochimica et Cosmochimica*

731 *Acta* , 300, 258-278. https://doi.org/10.1016/j.gca.2021.02.034

732 Appelo, C. A. J., Van Loon, L. R., & Wersin, P. (2010). Multicomponent diffusion of a suite of

733 tracers (HTO, Cl, Br, I, Na, Sr, Cs) in a single sample of Opalinus Clay. Geochimica et

734 Cosmochimica Acta, 74(4), 1201-1219.

735 Bagheri, R., Nadri, A., Raeisi, E., Eggenkamp, H. G. M., Kazemi, G. A., & Montaseri, A.

736 (2014). Hydrochemical and isotopic ($\delta^{18}O$, δ^2H, $^{87}Sr/^{86}Sr$, $\delta^{37}Cl$ and $\delta^{81}Br$) evidence for the

737 origin of saline formation water in a gas reservoir. *Chemical Geology*, *384*, 62-75.

738 Bahnan, A. E., Carpentier, C., Pironon, J., Ford, M., Ducoux, M., Barré, G., ... & Gaucher, E. C.

739 (2020). Impact of geodynamics on fluid circulation and diagenesis of carbonate reservoirs in a

740 foreland basin: Example of the Upper Lacq reservoir (Aquitaine basin, SW France). *Marine*

741 *and Petroleum Geology*, *111*, 676-694.

742 Balan, E., Créon, L., Sanloup, C., Aléon, J., Blanchard, M., Paulatto, L., & Bureau, H. (2019).

743 First-principles modeling of chlorine isotope fractionation between chloride-bearing

744 molecules and minerals. *Chemical Geology*, *525*, 424-434.

745 Beekman, H. E., Eggenkamp, H. G. M., & Appelo, C. A. J. (2011). An integrated modelling

746 approach to reconstruct complex solute transport mechanisms–Cl and $\delta^{37}Cl$ in pore water of

747   sediments from a former brackish lagoon in The Netherlands. *Applied geochemistry*, *26*(3),

748   257-268.

749 Bernachot, I., Garcia, B., Ader, M., Peysson, Y., Rosenberg, E., Bardoux, G., & Agrinier, P.

750   (2017). Solute transport in porous media during drying: The chlorine isotopes point of view.

751   *Chemical Geology*, *466*, 102-115.

752 Bethke, C. M., & Marshak, S. (1990). Brine migrations across North America—The plate

753   tectonics of groundwater. *Annual Review of Earth and Planetary Sciences*, *18*(1), 287-315.

754 Bolt, G.H. and De Haan, F.A.M. (1982) Anion exclusion in soil. In: Bolt, G.H. (Ed.), Soil

755   Chemistry: B. Physico-chemical Models. Elsevier, Amsterdam.

756 Bons, P. D., & Gomez-Rivas, E. (2013). Gravitational fractionation of isotopes and dissolved

757   components as a first-order process in crustal fluids. *Economic Geology*, *108*(5), 1195-1201.

758 Bourg, I. C., Sposito, G., & Bourg, A. (2006). Tracer diffusion in compacted, water-saturated

759   bentonite. *Clays and Clay Minerals*, *54*(3), 363-374.

760 Bozau, E., Sattler, C. D., & van Berk, W. (2015). Hydrogeochemical classification of deep

761   formation waters. *Applied Geochemistry*, *52*, 23-30.

762 Bradbury, M. H., & Baeyens, B. (1998). A physicochemical characterisation and geochemical

763   modelling approach for determining porewater chemistries in argillaceous rocks. *Geochimica

764   et Cosmochimica Acta*, *62*(5), 783-795.

765 Bradbury, M. H., & Baeyens, B. (2003). Porewater chemistry in compacted re-saturated MX-80

766   bentonite. *Journal of Contaminant Hydrology*, *61*(1-4), 329-338.

767 Brady, N. C., Weil, R. R., & Weil, R. R. (2008). *The nature and properties of soils* (Vol. 13, pp.

768   662-710). Upper Saddle River, NJ: Prentice Hall.

769 Brigatti, M. F., Galan, E., & Theng, B. K. G. (2013). Structure and mineralogy of clay minerals.

770   In *Developments in clay science* (Vol. 5, pp. 21-81). Elsevier.

771 Campbell, D. J. (1985). *FRACTIONATION OF STABLE CHLORINE ISOTOPES DURING

772   TRANSPORT THROUGH SEMIPERMEABLE MEMBRANES* (Doctoral dissertation, The

773   University of Arizona).

774 Carpenter, A. B. (1978, October). Origin and chemical evolution of brines in sedimentary basins.

775   In *SPE Annual Fall Technical Conference and Exhibition*. OnePetro.

776 Celejewski, M., Barton, D., & Al, T. (2018). Measurement of Cl−: Br− Ratios in the Porewater

777   of Clay-Rich Rocks—A Comparison of the Crush-and-Leach and the Paper-Absorption

778   Methods. *Geofluids*, *2018*.

779 Coleman, M. L. (1992). Water composition variation within one formation. In *International

780   symposium on water-rock interaction* (pp. 1109-1112).

34

781 Coplen, T. B., & Hanshaw, B. B. (1973). Ultrafiltration by a compacted clay membrane—I.

782   Oxygen and hydrogen isotopic fractionation. *Geochimica et Cosmochimica Acta*, *37*(10),

783   2295-2310.

784 Davis, S. N., Whittemore, D. O., & Fabryka-Martin, J. (1998). Uses of chloride/bromide ratios in

785   studies of potable water. *Groundwater*, *36*(2), 338-350.

786 Demir, I. (1988). Studies of smectite membrane behavior Electrokinetic, osmotic, and isotopic

787   fractionation processes at elevated pressures. *Geochimica et Cosmochimica Acta*, *52*(3), 727-

788   737.

789 Desaulniers, D. E., Kaufmann, R. S., Cherry, J. A., & Bentley, H. W. (1986). ^{37}Cl-^{35}Cl variations

790   in a diffusion-controlled groundwater system. *Geochimica et Cosmochimica Acta*, *50*(8),

791   1757-1764.

792 Descostes, M., Blin, V., Bazer-Bachi, F., Meier, P., Grenut, B., Radwan, J., ... & Tevissen, E.

793   (2008). Diffusion of anionic species in Callovo-Oxfordian argillites and Oxfordian limestones

794   (Meuse/Haute–Marne, France). *Applied Geochemistry*, *23*(4), 655-677.

795 Eggenkamp, H. G. M. (1994). $\delta^{37}Cl$: The geochemistry of chlorine isotopes (Ph. D. thesis,

796   Utrecht, Universiteit Utrecht).

797 Eggenkamp, H. G. M. (2014)a. A closer look at chlorine and bromine isotopes; An approach to

798   understand the similarities and differences. *Journal of Biology and Earth Sciences*, *4*.

799 Eggenkamp, H. (2014)b. *The geochemistry of stable chlorine and bromine isotopes* (pp. 127-

800   130). Berlin: Springer.

801 Eggenkamp, H. G. M., Bonifacie, M., Ader, M., & Agrinier, P. (2016). Experimental

802   determination of stable chlorine and bromine isotope fractionation during precipitation of salt

803   from a saturated solution. *Chemical Geology*, *433*, 46-56.

804 Eggenkamp, H. G. M., & Coleman, M. L. (2009). The effect of aqueous diffusion on the

805   fractionation of chlorine and bromine stable isotopes. *Geochimica et Cosmochimica Acta*,

806   *73*(12), 3539-3548.

807 Eggenkamp, H. G. M., Kreulen, R., & Van Groos, A. K. (1995). Chlorine stable isotope

808   fractionation in evaporites. *Geochimica et Cosmochimica Acta*, *59*(24), 5169-5175.

809 Eggenkamp, H. G. M., Bonifacie, M., Ader, M., & Agrinier, P. (2016). Experimental

810   determination of stable chlorine and bromine isotope fractionation during precipitation of salt

811   from a saturated solution. *Chemical Geology*, *433*, 46-56.

812 Eggenkamp, H. G. M., & Louvat, P. (2018). A simple distillation method to extract bromine

813   from natural water and salt samples for isotope analysis by multi-collector inductively

814   coupled plasma mass spectrometry. *Rapid Communications in Mass Spectrometry*, *32*(8),

815   612-618.

816 Eggenkamp, H. G. M., Louvat, P., Agrinier, P., Bonifacie, M., Bekker, A., Krupenik, V., ... &

817   Bagheri, R. (2019). The bromine and chlorine isotope composition of primary halite deposits

818   and their significance for the secular isotope composition of seawater. *Geochimica et*

819   *Cosmochimica Acta*, *264*, 13-29.

820 Fontes J.C. & Mantray J.M. (1993) Geochemistry and origin of formation brines from the Paris

821   Basin, France; 1. Brines associated with Triassic salts. Chem. Geol. 109, 149-175.

822 Garven, G. (1995). Continental-scale groundwater flow and geologic processes. *Annual Review*

823   *of Earth and Planetary Sciences*, *23*(1), 89-117.

824 Godon A., Jendrzejewski N., Eggenkamp H. G. M., Banks D. A., Ader M., Coleman M. L. and

825   Pineau F. (2004) A crosscalibration of chlorine isotopic measurements and suitability of

826   seawater as the international reference material. *Chemical Geology*, 207(1-2), 1–12.

827 Hanor, J. S., & Hanor, J. S. (1987). Origin and migration of subsurface sedimentary brines.

828 Haydon, P. R., & Graf, D. L. (1986). Studies of smectite membrane behavior: temperature

829   dependence, 20–180° C. *Geochimica et Cosmochimica Acta*, *50*(1), 115-121.

830 Hendry, M. J., Wassenaar, L. I., & Kotzer, T. (2000). Chloride and chlorine isotopes (^{36}Cl and

831   δ^{37}Cl) as tracers of solute migration in a thick, clay-rich aquitard system. *Water Resources*

832   *Research*, *36*(1), 285-296.

833 Hesse, R., Egeberg, P. K., & Frape, S. K. (2006). Chlorine stable isotope ratios as tracer for

834   pore-water advection rates in a submarine gas-hydrate field: implication for hydrate

835   concentration. *Geofluids*, *6*(1), 1-7.

836 Karnland, O., Olsson, S., Nilsson, U., & Sellin, P. (2007). Experimentally determined swelling

837   pressures and geochemical interactions of compacted Wyoming bentonite with highly alkaline

838   solutions. *Physics and Chemistry of the Earth, Parts A/B/C*, *32*(1-7), 275-286.

839 Kaufmann, R., Long, A., Bentley, H., & Davis, S. (1984). Natural chlorine isotope variations.

840   *Nature*, *309*(5966), 338-340.

841 Kendrick, M. A., Phillips, D., Wallace, M., & Miller, J. M. (2011). Halogens and noble gases in

842   sedimentary formation waters and Zn–Pb deposits: A case study from the Lennard Shelf,

843   Australia. *Applied Geochemistry*, *26*(12), 2089-2100.

844 Kharaka, Y. K., & Berry, F. A. (1973). Simultaneous flow of water and solutes through

845   geological membranes—I. Experimental investigation. *Geochimica et Cosmochimica Acta*,

846   *37*(12), 2577-2603.

847 Kharaka Y.K. & Hanor J.S. (2003). Deep fluids in the continents: I. Sedimentary basins. In:

848   Drever, J.I., Holland, H.D., Turekian, K.K. (Eds.), Treatise in Geochemistry 5, 499–540.

849 Kozaki, T., Saito, N., Fujishima, A., Sato, S., & Ohashi, H. (1998). Activation energy for

850   diffusion of chloride ions in compacted sodium montmorillonite. *Journal of Contaminant*

851   *Hydrology*, *35*(1-3), 67-75.

852 Langmuir, I. (1918). The adsorption of gases on plane surfaces of glass, mica and platinum.

853   *Journal of the American Chemical society*, *40*(9), 1361-1403.

854 Lavastre, V., Jendrzejewski, N., Agrinier, P., Javoy, M., & Evrard, M. (2005). Chlorine transfer

855   out of a very low permeability clay sequence (Paris Basin, France): ^{35}Cl and ^{37}Cl evidence.

856   *Geochimica et Cosmochimica Acta*, *69*(21), 4949-4961.

857 Lindemann, F. A. (1921). In discussion of isotopes. *Proc. Roy. Soc. Lond. Ser. A*, *99*, 102-104.

858 Louvat, P., Bonifacie, M., Giunta, T., Michel, A., & Coleman, M. (2016). Determination of

859   bromine stable isotope ratios from saline solutions by "wet plasma" MC-ICPMS Including a

860   comparison between high-and low-resolution modes, and three introduction systems.

861   *Analytical chemistry*, *88*(7), 3891-3898.

862 Luo, C., Xiao, Y., Wen, H., Ma, H., Ma, Y., Zhang, Y., ... & He, M. (2014). Stable isotope

863   fractionation of chlorine during the precipitation of single chloride minerals. *Applied*

864   *geochemistry*, *47*, 141-149.

865 Melkior, T., Gaucher, E. C., Brouard, C., Yahiaoui, S., Thoby, D., Clinard, C., ... & Coelho, D.

866   (2009). Na+ and HTO diffusion in compacted bentonite: Effect of surface chemistry and

867   related texture. *Journal of Hydrology*, *370*(1-4), 9-20.

868 Molera, M., & Eriksen, T. (2002). Diffusion of ^{22}Na$^+$, ^{85}Sr^{2+}, ^{134}Cs$^+$ and ^{57}Co^{2+} in bentonite clay

869   compacted to different densities: experiments and modeling. *Radiochimica Acta*, *90*(9-11),

870   753-760.

871 Mondol, N. H., Bjørlykke, K., Jahren, J., & Høeg, K. (2007). Experimental mechanical

872   compaction of clay mineral aggregates—Changes in physical properties of mudstones during

873   burial. *Marine and petroleum geology*, *24*(5), 289-311.

874 Musashi, M., Oi, T., & Eggenkamp, H. G. (2004). Experimental determination of chlorine

875   isotope separation factor by anion-exchange chromatography. *Analytica chimica acta*, *508*(1),

876   37-40.

877 Muurinen, A., Karnland, O., & Lehikoinen, J. (2004). Ion concentration caused by an external

878   solution into the porewater of compacted bentonite. *Physics and Chemistry of the Earth, Parts*

879   *A/B/C*, *29*(1), 119-127.

880 Nakata, K., Hasegawa, T., Higashihara, T., & Oyama, T. (2016). Chloride ion concentrations

881   during the compression of rocks to extract pore water. *Geofluids*, *16*(1), 78-88.

882 Neaman, A., Pelletier, M., & Villieras, F. (2003). The effects of exchanged cation, compression,

883   heating and hydration on textural properties of bulk bentonite and its corresponding purified

884   montmorillonite. *Applied Clay Science*, *22*(4), 153-168.

885 Neuzil, C. E., & Person, M. (2017). Reexamining ultrafiltration and solute transport in

886   groundwater. *Water Resources Research*, *53*(6), 4922-4941.

887 Nygård, R., Gutierrez, M., Gautam, R., & Høeg, K. (2004). Compaction behavior of argillaceous

888   sediments as function of diagenesis. *Marine and Petroleum Geology*, *21*(3), 349-362.

889 Phillips, F. M., & Bentley, H. W. (1987). Isotopic fractionation during ion filtration: I. Theory.

890   *Geochimica et Cosmochimica Acta*, *51*(3), 683-695.

891 Plecis, A., Schoch, R. B., & Renaud, P. (2005). Ionic transport phenomena in nanofluidics:

892   experimental and theoretical study of the exclusion-enrichment effect on a chip. *Nano letters*,

893   *5*(6), 1147-1155.

894 Pusch, R., Karnland, O., & Hökmark, H. (1990). *GMM-a general microstructural model for*

895   *qualitative and quantitative studies of smectite clays* (No. SKB-TR--90-43). Swedish Nuclear

896   Fuel and Waste Management Co.

897 Revil, A., & Leroy, P. (2004). Constitutive equations for ionic transport in porous shales.

898   *Journal of Geophysical Research: Solid Earth*, *109*(B3).

899 Richard, A., Banks, D. A., Mercadier, J., Boiron, M. C., Cuney, M., & Cathelineau, M. (2011).

900   An evaporated seawater origin for the ore-forming brines in unconformity-related uranium

901   deposits (Athabasca Basin, Canada): Cl/Br and δ^{37}Cl analysis of fluid inclusions.

902   *Geochimica et Cosmochimica Acta*, *75*(10), 2792-2810.

903 Richard, A., Kendrick, M. A., & Cathelineau, M. (2014). Noble gases (Ar, Kr, Xe) and halogens

904   (Cl, Br, I) in fluid inclusions from the Athabasca Basin (Canada): Implications for

905   unconformity-related U deposits. Precambrian Research 247, 110-125.

906 Richet, P., Bottinga, Y., & Javoy, M. (1977). A review of hydrogen, carbon, nitrogen, oxygen,

907   sulphur, and chlorine stable isotope fractionation among gaseous molecules. *Annual Review*

908   *of Earth and Planetary Sciences*, *5*(1), 65-110.

909 Sato, H., Ashida, T., Kohara, Y., Yui, M., & Sasaki, N. (1992). Effect of dry density on diffusion

910   of some radionuclides in compacted sodium bentonite. *Journal of Nuclear Science and*

911   *Technology*, *29*(9), 873-882.

912 Sauzeat, E., Guillaume, D., Neaman, A., Dubessy, J., François, M., Pfeiffert, C., ... &

913   Cathelineau, M. (2001). Caractérisation minéralogique, cristallochimique et texturale de

914   l'argile MX80, Rapport ANDRA No. *RP. 0LEM*, 01-001.

915 Schauble, E. A. (2004). Applying stable isotope fractionation theory to new systems. *Reviews in

916   mineralogy and geochemistry*, *55*(1), 65-111.

917 Schauble, E. A., Rossman, G. R., & Taylor Jr, H. P. (2003). Theoretical estimates of equilibrium

918   chlorine-isotope fractionations. *Geochimica et Cosmochimica Acta*, *67*(17), 3267-3281.

919 Shackelford, C. D., & Daniel, D. E. (1991). Diffusion in saturated soil. II: Results for compacted

920   clay. *Journal of Geotechnical Engineering*, *117*(3), 485-506.

921 Shirodkar, P. V., Xiao, Y. K., & Hai, L. (2003). Boron and chlorine isotopic signatures of

922   seawater in the Central Indian Ridge. *Current Science*, 313-320.

923 Shouakar-Stash, O., Alexeev, S. V., Frape, S. K., Alexeeva, L. P., & Drimmie, R. J. (2007).

924   Geochemistry and stable isotopic signatures, including chlorine and bromine isotopes, of the

925   deep groundwaters of the Siberian Platform, Russia. *Applied geochemistry*, *22*(3), 589-605.

926 Solley, W. B., & Chase, E. B. (1983). Estimated use of water in the United States in 1980.

927 Stotler, R. L., Frape, S. K., & Shouakar-Stash, O. (2010). An isotopic survey of $\delta^{81}Br$ and $\delta^{37}Cl$

928   of dissolved halides in the Canadian and Fennoscandian Shields. *Chemical Geology*, *274*(1-

929   2), 38-55.

930 Tournassat, C., & Appelo, C. A. J. (2011). Modelling approaches for anion-exclusion in

931   compacted Na-bentonite. *Geochimica et Cosmochimica Acta*, *75*(13), 3698-3710.

932 Tremosa, J., Gailhanou, H., Chiaberge, C., Castilla, R., Gaucher, E. C., Lassin, A., ... & Claret,

933   F. (2020). Effects of smectite dehydration and illitisation on overpressures in sedimentary

934   basins: A coupled chemical and thermo-hydro-mechanical modelling approach. *Marine and

935   Petroleum Geology*, *111*, 166-178.

936 Urey, H. C. (1947). The thermodynamic properties of isotopic substances. *Journal of the

937   Chemical Society (Resumed)*, 562-581.

938 Van Loon, L. R., Glaus, M. A., & Müller, W. (2007). Anion exclusion effects in compacted

939   bentonites: towards a better understanding of anion diffusion. *Applied Geochemistry*, *22*(11),

940   2536-2552.

941 Van Loon, L. R., Soler, J. M., Müller, W., & Bradbury, M. H. (2004). Anisotropic diffusion in

942   layered argillaceous rocks: a case study with Opalinus Clay. *Environmental science &

943   technology*, *38*(21), 5721-5728.

944 Wersin, P., Curti, E., & Appelo, C. A. J. (2004). Modelling bentonite–water interactions at high

945   solid/liquid ratios: swelling and diffuse double layer effects. *Applied Clay Science*, *26*(1-4),

946   249-257.

947 Wigger, C., & Van Loon, L. R. (2017). Importance of interlayer equivalent pores for anion

948   diffusion in clay-rich sedimentary rocks. *Environmental science & technology*, *51*(4), 1998-

949   2006.

950 Worden, R. H. (1996). Controls on halogen concentrations in sedimentary formation waters.

951   *Mineralogical Magazine*, *60*(399), 259-274.

952 Zhang, T., & Krooss, B. M. (2001). Experimental investigation on the carbon isotope

953   fractionation of methane during gas migration by diffusion through sedimentary rocks at

954   elevated temperature and pressure. *Geochimica et Cosmochimica Acta*, *65*(16), 2723-2742.

Clay compaction leads to expelled water freshening

Clay compaction leads to Cl and Br isotopes fractionation

Ultrafiltration is more effective for clay with the more negative surface charge

The retention effect in clay porosity is slightly more pronounced for Br than for Cl

Declaration of interests

☒ The authors declare that they have no known competing financial interests or personal relationships that could have appeared to influence the work reported in this paper.

☐The authors declare the following financial interests/personal relationships which may be considered as potential competing interests: